


No Pulsar Left Behind. I. Timing, Pulse-sequence Polarimetry, and Emission Morphology for 12 pulsars.

Casey Brinkman,¹  Paulo C. C. Freire,² Joanna Rankin^{1,3} and Kevin Stovall⁴

¹*Physics Department, University of Vermont, Burlington, Vermont 05401, USA*

²*Max-Planck-Institut für Radioastronomie, auf dem Hügel 69, 53121 Bonn, Germany*

³*Anton Pannekoek Institute for Astronomy, University of Amsterdam, Science Park 904, 1098 XH Amsterdam*

⁴*National Radio Astronomy Observatory, P.O. Box 0, Socorro, NM 87801, USA*

Accepted XXX. Received YYY; in original form ZZZ

ABSTRACT

In this paper we study a set of twelve pulsars that previously had not been characterized. Our timing shows that eleven of them are “normal” isolated pulsars, with rotation periods between 0.22 and 2.65 s, characteristic ages between 0.25 Myr and 0.63 Gyr, and estimated magnetic fields ranging from 0.05 to 3.8×10^{12} G. The youngest pulsar in our sample, PSR J0627+0706, is located near the Monoceros supernova remnant (SNR G205.5+0.5), but it is not the pulsar most likely to be associated with it. We also confirmed the existence of a candidate from an early Arecibo survey, PSR J2053+1718, its subsequent timing and polarimetry are also presented here. It is an isolated pulsar with a spin period of 119 ms, a relatively small magnetic field of 5.8×10^9 G and a characteristic age of 6.7 Gyr; this suggests the pulsar was mildly recycled by accretion from a companion star which became unbound when that companion became a supernova. We report the results of single-pulse and average Arecibo polarimetry at both 327 and 1400 MHz aimed at understanding the basic emission properties and beaming geometry of these pulsars. Three of them (PSRs J0943+2253, J1935+1159 and J2050+1259) have strong nulls and sporadic radio emission, several others exhibit interpulses (PSRs J0627+0706 and J0927+2345) and one shows regular drifting subpulses (J1404+1159).

Key words: pulsars: general, pulsars: individual: PSR J0627+0706, pulsars: individual: PSR J2053+1718, astrometry: polarization

1 INTRODUCTION AND MOTIVATION

Since the discovery of the first radio pulsar in 1967 (Hewish et al. 1968), more than 2500 rotation-powered pulsars have been discovered (Manchester et al. 2005). Of these, more than 400 have been “left behind”—that is, they have no published phase-coherent timing solutions, so that we lack a rudimentary knowledge of their proper motions, spin-down parameters (including characteristic age, magnetic field, spin-down luminosity) and possible orbital elements. Similarly, no polarimetry and fluctuation-spectral analyses have been done for many pulsars, and for many of these even basic quantities such as flux densities, rotation measures and spectral indices are lacking. Because of this, the scientific potential for many of these objects is simply unknown and unexploited.

In this and subsequent papers, we attempt a partial remedy to this situation by characterizing some of these

pulsars: we present their timing solutions (with derivations of characteristic ages, surface magnetic field and rotational spin-down) and study some of their radio emission properties. As for all previously well characterized pulsars, the measurements presented here and in subsequent papers will aid future studies of the pulsar population and contribute to the understanding of their emission physics.

In this first paper, we focus on a group of a dozen pulsars discovered with the 430-MHz line feed of the Arecibo 305-m radio telescope in Puerto Rico *before* the Arecibo upgrade, i.e., pulsars that were found more than 20 years ago, but were then never followed up. Most pulsars in this group were discovered in drift-scan surveys: two, J0943+22 and J1246+22, were reported by Thorsett et al. (1993) and three others (J0435+27, J0927+23, J0947+27) were discovered in the completion of that survey by Ray et al. (1996). Five further pulsars (J0517+22, J0627+07, J1404+12, J1935+12 and J1938+22) were discovered in the Arecibo-Caltech drift-scan survey (Chandler 2003), but again no timing solutions were presented for any of them. Two of these pulsars were

* E-mail: clbrinkm@uvm.edu

Previous name	Reference	New Name	Start (MJD)	Finish (MJD)	NTOA	rms (ms)	Reduced χ^2
J0435+27	Ray et al. (1996)	J0435+2749	52854	53785	96	0.12	14.38
J0517+22	Chandler (2003)	J0517+2212	53418	57701	518	0.12	7.9
J0627+07*	Chandler (2003)	J0627+0706	53418	53675	91	0.26	22.82
J0927+23	Ray et al. (1996)	J0927+2345	53318	53910	26	0.47	0.77
J0943+22	Thorsett et al. (1993)	J0943+2253	53318	57876	731	0.17	2.57
J0947+27	Ray et al. (1996)	J0947+2740	53318	53910	35	0.28	1.88
J1246+22	Thorsett et al. (1993)	J1246+2253	53294	57876	448	0.22	4.28
J1404+12	Chandler (2003)	J1404+1159	53309	57380	335	0.62	12.78
J1756+18	Navarro et al. (2003)	J1756+1822	52645	53307	89	1.23	26.09
J1935+12	Chandler (2003)	J1935+1159	53306	57504	145	2.51	1.04
J2050+13	Navarro et al. (2003)	J2050+1259	52636	53306	27	8.81	1419.67
J2052+17**	Ray et al. (1996)	J2053+1718	53295	56837	728	0.028	1.34

Table 1. Pulsar names (old and new), references and the parameters of our timing observations. *See also Burgay et al. (2013) **Previous unconfirmed candidate.

later timed by other authors: J0627+0706, which we timed from 2005 Feb. 17 to Nov. 1, was detected by the Perseus Arm pulsar survey and subsequently timed from 2006 Jan 1 to 2011 May 9 (Burgay et al. 2013). Their timing results are similar to ours, but more precise given the larger timing baseline. J1938+22, which we did not follow up, was later timed by Lorimer et al. (2013), so that it is now known as J1938+2213.

Two other pulsars (J1756+18 and J2050+13) were discovered in the Arecibo 430-MHz intermediate latitude (pointed) survey (Navarro et al. 2003). They were reported in the above paper describing that survey, but without timing solutions because although they were originally detected on the 19th and 13th of July 1990 respectively, they were confirmed only in January 2003.

Finally, in Ray et al. (1996) an additional pulsar candidate (J2052+17) was listed, but the authors were unable to confirm it because of the start of the Arecibo upgrade. The candidate had a spin period P of 119.26 ms and a DM of $25 \pm 3 \text{ cm}^{-3} \text{ pc}$. In 2004 October we confirmed the existence of this pulsar using the 327 MHz Gregorian receiver of the 305-m Arecibo radio telescope and the Wideband Arecibo Pulsar Processors (WAPPs, Dowd et al. 2000) as back-ends. Both the topocentric spin period (119.27 ms) and DM of $27 \text{ cm}^{-3} \text{ pc}$ were compatible with the parameters in Ray et al. (1996). The pulsar has an exceptionally narrow profile, which represents less than 1% of a rotation cycle as presented in Fig. 1 and in more detail in Fig. 14.

In what follows, we present detailed studies for these objects, both of their timing and emission properties. In §2 we discuss briefly the timing observations and their results, §3 describes the pulse-sequence, profile and polarization analyses, §4 discusses the origin of PSR J2053+1718 and §5 summarizes the various results.

2 TIMING OBSERVATIONS AND RESULTS

The aforementioned pulsars are relatively bright, and for that reason were used as test pulsars during the very early demonstration stages of the Arecibo 327-MHz drift scan survey (AO327, Deneva et al. 2013). These observations were carried out with the 327-MHz Gregorian feed and one of the four WAPPs as backends. They all were acquired in search

mode, with 256 spectral channels, a sampling time of $64 \mu\text{s}$ and a bandwidth of 50 MHz. They were later dedispersed and folded using the PRESTO routine “prepfold” (Ransom et al. 2002), and then topocentric pulse times of arrival (TOAs) were derived from the resulting profiles using the FFT technique described by Taylor (1992) and implemented in the PRESTO routine `get_TOAs.py`.

At a later phase (2015/2016), we have used some of these pulsars (J0517+2212, J0943+2253, J1246+2253, J1404+1159 and J1935+1159) as test pulsars during follow-up sessions of AO327 discovered pulsars. These observations were made using the same 327-MHz Gregorian feed, but with the Puerto Rican Ultimate Pulsar Processing Instrument (PUPPI), which is a clone of the Greenbank Ultimate Pulsar Processing Instrument (GUPPI)¹. Initial observations consisted of incoherent search mode observations with 69 MHz of bandwidth that was split into 2816 channels with a sample time of $81.92 \mu\text{s}$. These data were dedispersed and folded using the `fold_psrfits` routine from the `psrfits_utils` software package². Later observations were performed using PUPPI in coherent fold mode with the same 69 MHz of bandwidth split into 44 frequency channels and were written to disk every 10 s. RFI was excised from both incoherent and coherent PUPPI files using a median-zapping algorithm included in the PSRCHIVE software package (van Straten et al. 2012)³ and topocentric TOAs were derived using PSRCHIVE’s `pat` tool.

The TOAs were then analyzed using `tempo`⁴, with the DE405 solar system ephemeris⁵; from this we derive a timing solution, where we can assign the correct integer rotation number to each pulse.

The characteristics of the timing observations are given in Table 1, together with the number of TOAs derived for each, the root mean square (rms) of the residuals (a residual

¹ <https://safe.nrao.edu/wiki/bin/view/CICADA/GUPPIUsersGuide>

² http://github.com/scottransom/psrfits_utils

³ <http://psrchive.sourceforge.net/>

⁴ <http://tempo.sourceforge.net/>

⁵ Standish, E.M.: 1998, “JPL Planetary and Lunar Ephemerides, DE405/LE405”, <ftp://ssd.jpl.nasa.gov/pub/eph/planets/ioms/de405.iom.pdf>

Pulsar Name	Right Ascension hh mm ss.ss	Declination ° ' "	ν (Hz)	$\dot{\nu}$ (10^{-16} Hz s $^{-1}$)	DM (pc cm $^{-3}$)
J0435+2749	04 35 51.818(4)	27 49 01.7(4)	3.064857408039(13)	-0.767(10)	53.19(2)
J0517+2212	05 17 17.147(2)	22 12 51.9(2)	4.497079963269(13)	-2.3469(3)	18.705(14)
J0627+0706	06 27 44.217(2)	07 06 12.7(11)	2.1013960823(5)	-1314.8(4)	138.29
J0927+2345	09 27 45.26(5)	23 45 10.7(12)	1.31252674625(15)	-5.26(6)	17.24(12)
J0943+2253	09 43 32.3975(10)	22 53 05.66(4)	1.876261648496(3)	-3.16238(7)	27.2508(15)
J0947+2740	09 47 21.287(18)	27 40 43.5(2)	1.17506907189(7)	-5.94(3)	29.09(7)
J1246+2253	12 46 49.363(5)	22 53 43.27(8)	2.110280928271(14)	-3.9586(4)	17.792(3)
J1404+1159	14 04 36.961(3)	11 59 15.36(10)	0.377296025592(4)	-1.95656(16)	18.466(9)
J1756+1822	17 56 17.583(8)	18 22 55.3(2)	1.34408432377(12)	-9.27(3)	70.80
J1935+1159	19 35 16.076(14)	11 59 09.2(4)	0.51552817782(4)	-2.5190(15)	188.76(6)
J2050+1259	20 50 57.21(14)	12 59 09(3)	0.8189874162(6)	-3.38(15)	52.40
J2053+1718	20 53 49.4809(7)	17 18 44.662(13)	8.384495643240(8)	-0.2014(7)	26.979

Table 2. Parameters from the timing solution for the reference epoch MJD = 53400. The digits in parentheses indicate the $1\text{-}\sigma$ uncertainty estimated by `tempo` on the last digit of the value.

Pulsar Name	Galactic Coord.		P	\dot{P}	$\log_{10}(\tau_c)$	$\log_{10}(B_0)$	D_1	D_2	$\log_{10}\dot{E}$
	l	b	(s)	(10^{-15} s s $^{-1}$)	(τ_c in yr)	(B_0 in G)	(kpc)	(kpc)	(\dot{E} in erg s $^{-1}$)
J0435+2749	171.8	-13.1	0.3262794534509(14)	0.00816(11)	8.8	10.7	1.8	1.5	31.0
J0517+2212	182.2	-9.0	0.2223665151983(6)	0.0116045(15)	8.5	10.7	0.66	0.16	31.5
J0627+0706	203.9	-2.0	0.47587411455(11)	29.775(9)	5.4	12.6	4.7	2.3	34.0
J0927+2345	205.3	+44.2	0.76188923606(9)	0.305(4)	7.6	11.7	0.66	1.1	31.4
J0943+2253	207.9	+47.5	0.5329747057409(7)	0.089831(2)	8.0	11.3	1.2	3.5	31.4
J0947+2740	201.1	+49.4	0.85101380330(5)	0.430(2)	7.5	11.8	1.28	*	31.4
J1246+2253	288.8	+85.6	0.473870557518(3)	0.088891(9)	7.9	11.3	1.5	2.5	31.5
J1404+1159	355.1	+67.1	2.65043873291(3)	1.37445(11)	7.5	12.3	1.4	2.2	30.4
J1756+1822	43.8	+20.2	0.74400093976(6)	0.5129(16)	7.4	11.8	4.2	*	31.7
J1935+1159	48.6	-4.1	1.93975818009(15)	0.9478(6)	7.5	12.1	6.8	8.7	30.7
J2050+1259	59.4	-19.2	1.2210199817(9)	0.50(2)	7.6	11.9	3.1	5.9	31.0
J2053+1718	63.6	-17.3	0.11926775831845(11)	0.0002864(10)	9.8	9.8	1.9	2.1	30.8

Table 3. Derived parameters. The digits in parentheses indicate the $1\text{-}\sigma$ uncertainty estimated by `tempo` on the last digit of the value. D_1 is calculated using the NE2001 model, D_2 is calculated using the YMW16 model. The asterisks indicate that the DM is larger than the model prediction for the total Galactic column density for the pulsar’s line of sight.

is the measured TOA minus the prediction of the timing solution for the time of the respective pulse). As an example, we depict graphically the residuals of PSR J2053+1718 in Fig. 2) and the reduced χ^2 of each fit. For some pulsars this is much larger than 1, implying either the presence of effects that have not been modelled in their timing solutions, such as timing noise or pulse jitter, or that for some reason the TOA uncertainties were greatly under-estimated. The table also gives the new names for these pulsars, these names are used throughout the remainder of this paper.

The timing solutions themselves are presented in Table 2, these include precise measurements of Right Ascension and Declination (this is the origin of the new names in the preceding table) and in some cases the proper motion along these two directions (μ_α and μ_δ), the rotation frequency (ν), its derivative ($\dot{\nu}$), and dispersion measure (DM). The reference epoch for all timing parameters is MJD = 53400. For these measurements, we have multiplied the TOA uncertainties by the square root of the reduced χ^2 in Table 1, this yields a new reduced χ^2 of 1.0. This procedure results in conservative estimates of the uncertainties of the timing parameters. These might still be in error due to the presence of correlated noise in the TOAs, such as that produced by timing

noise; this is particularly important for PSRs J0627+0706, J1756+1822 and especially PSR J2050+1259.

Finally, the derived parameters are given in Table 3: Galactic coordinates (l, b) and distance (D), the latter is derived from the DM using two models of the electron distribution in the Galaxy (the NE2001 model, Cordes & Lazio 2002 and the YMW16 model, Yao et al. 2017), the spin period (P), its derivative (\dot{P}), the characteristic age (τ_c), magnetic field (B_0), and spin-down energy (\dot{E}). The expressions for these quantities were adopted from Lorimer & Kramer (2004): $\tau_c = P/(2\dot{P})$, $B = 3.2 \times 10^{19} \sqrt{P\dot{P}}$ and $\dot{E} = 4\pi^2 I \dot{P}/P^3$, where I is the moment of inertia of the neutron star, which is generally assumed to be 10^{45} g cm 2 . All pulsars in the list are isolated, and most of them belong to the “normal” group, with fairly typical rotation periods (between 0.22 and 2.65 s), characteristic ages (between 0.25 Myr and 0.63 Gyr) and B-fields (from 0.05 to 3.8×10^{12} G). We now discuss the characteristic of the two extreme objects in our sample.

2.1 PSR J0627+0706

With a characteristic age of only 250 kyr, PSR J0627+0706 is by far the most energetic object in this sample. This object

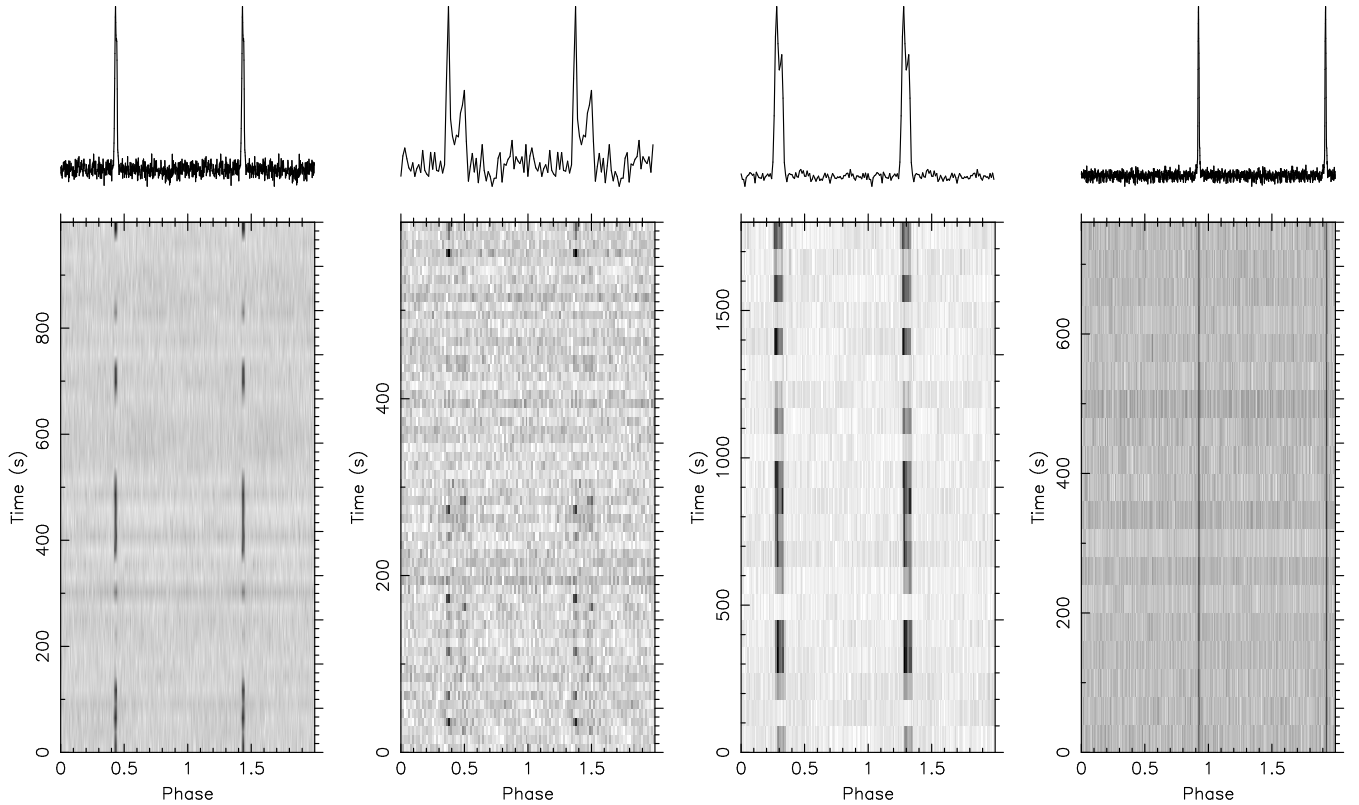


Figure 1. Gray-scaled intensity plots (with darker shade implying a larger intensity) showing total intensity of the pulsed signal at a frequency of 327 MHz as a function of spin phase (2 spin cycles shown for clarity) and time. During many time segments the pulsed signal of PSRs J0943+2253, J1935+1159 and J2050+1259 (but not PSR J2053+1718) disappears, i.e., the first three pulsars null. The right plot shows the remarkably narrow pulse profile of PSR J2053+1718.

displays a prominent interpulse, suggesting an orthogonal rotator. It also has significant timing noise, which is typical of young pulsars. This is the reason for the large reduced χ^2 of its solution. This agrees with the results of Burgay et al. (2013).

Chandler (2003) remarked that this pulsar lies, in projection, within 3° of the centre of the old, large Monoceros supernova remnant (SNR G205.5+0.5); which is located at an RA of $06^{\text{h}} 39^{\text{min}}$ and Declination of $+06^\circ 30'$. For this reason they proposed that, if PSR J0627+0706 has a true age similar to that of SNR G205.5+0.5 (30 to 100 kyr, Leahy et al. 1986), it could be a candidate in association with that SNR (they point out that the positional offset is possible given the age of the SNR and the proper motions of other pulsars observed in the Galaxy).

The characteristic age we and Burgay et al. (2013) measure for PSR J0627+0706 is larger by a factor of 2.5 to 8. However, this is not very constraining; true pulsar ages can be significantly smaller than their characteristic ages if they are born with a spin period similar to their current spin period.

Another way of verifying the association is through distance measurements. The estimated distance to the Monoceros SNR, 1.6 kpc (Odegard 1986), is smaller than the estimated DM distances to this pulsar, 4.5 kpc (NE 2001) and 2.3 kpc (YMW16). Given the uncertainties in the DM

models and their derived distances, this does not imply a distance inconsistency, particularly for the YMW16 model.

We note that this area of the Galaxy has an abundance of relatively young pulsars that could potentially be associated with SNR G205.5+0.5. In particular, the “radio quiet” gamma-ray pulsar PSR J0633+0632, discovered in data from the Fermi satellite (Abdo et al. 2009), was listed in the latter paper as a “plausible” association with SNR G205.5+0.5 based on its location within $\sim 1.5^\circ$ of the SNR centre. Later Ray et al. (2011) measured the characteristic age of PSR J0633+0632 (59 kyr) which is also more compatible with the estimated age of the SNR. However, the latter pulsar has yet no detected radio emission, so its DM (and derived distance) is not yet known.

Despite that, we conclude that PSR J0633+0632 is more likely to be associated to SNR G205.5+0.5 than PSR J0627+0706.

2.2 PSR J2053+1718

PSR J2053+1718 has a much smaller spin period derivative and a much larger characteristic age than the other pulsars in this sample. A first simple fit for the parameters in Table 2 plus proper motion (see below) yields a reduced χ^2 of 1.80, and visible trends in the residuals. Given the low frequency used in the timing and the relatively high precision of the measurements, these are likely due to variations

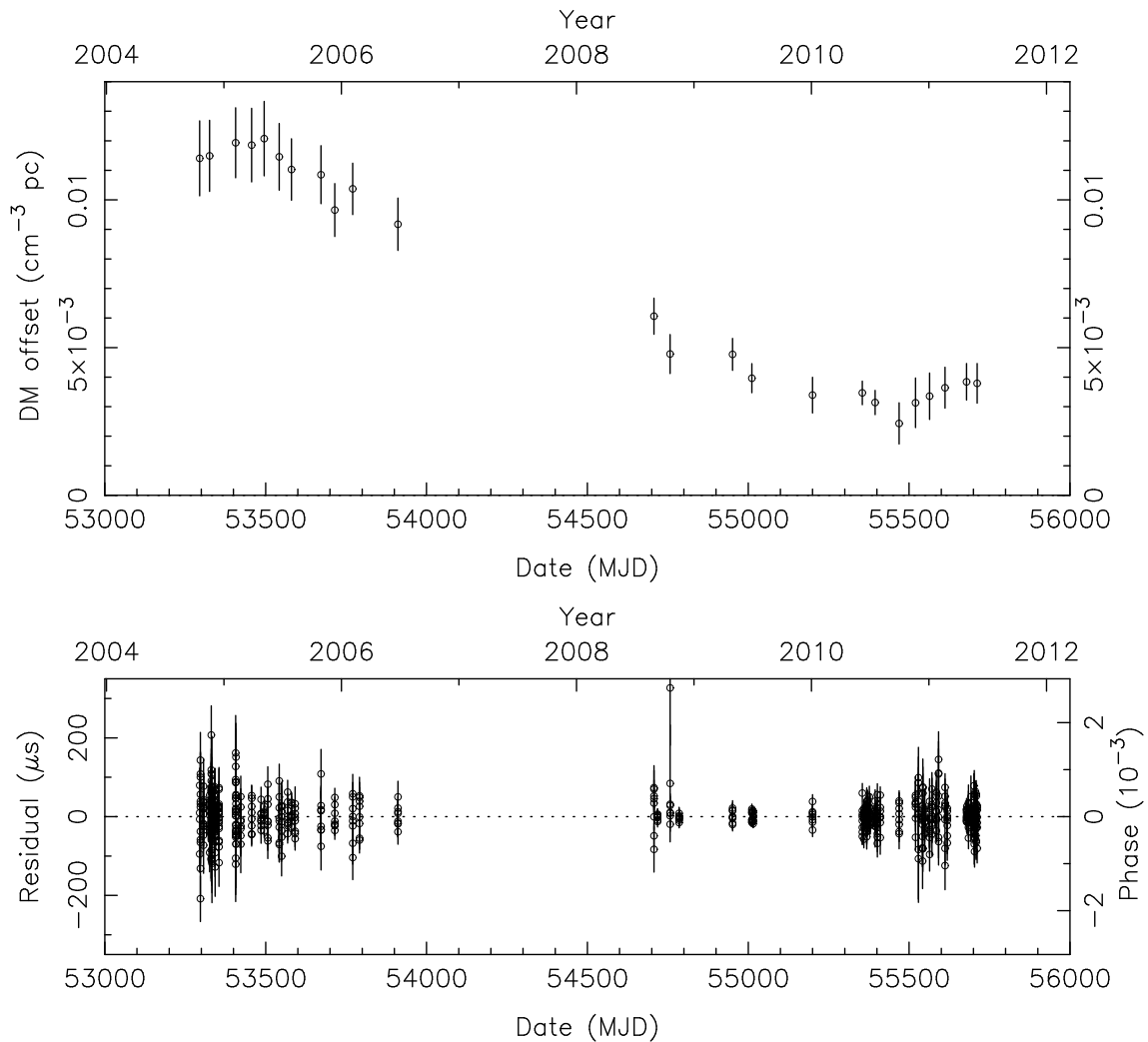


Figure 2. *Top plot:* Dispersion measure offset (from $26.979 \text{ cm}^{-3} \text{ pc}$) observed as a function of epoch for PSR J2053+1718. *Bottom plot:* Residuals as a function of epoch for the same pulsar. No trends are noticeable in the timing.

in DM caused by the Earth’s and the pulsar’s movement through space. In order to measure the DM variation with time, we divided the 50-MHz bandwidth in 4 sub-bands, making separate TOAs for each sub-band. We then used the DMX model (Demorest et al. 2013) to measure the DM variations (displayed in Fig. 2) and subtract them; once this is done the reduced χ^2 decreases to 1.34.

The precise timing of this pulsar allows a measurement of its proper motion in right ascension and declination: $\mu_\alpha = -1.0(23) \text{ mas yr}^{-1}$ and $\mu_\delta = +6.9(28) \text{ mas yr}^{-1}$. These measurements are not highly significant, but they already represent a significant constraint on the transverse velocity v_T . Given the DM distance estimates of 1.9 kpc (NE2001) and 2.1 kpc (YMW16), the proper motion implies $v_T = (63 \pm 25) \text{ km s}^{-1}$ and $(69 \pm 28) \text{ km s}^{-1}$ respectively; this is typical among recycled pulsars (e.g., Gonzalez et al. 2011).

This proper motion allows for a correction of the observed \dot{P} , where we subtract the Shklovskii effect (Shklovskii 1970) and the Galactic acceleration of this pulsar relative to that of the Solar System, projected along the line of sight (Damour & Taylor 1991) (this was calculated using the latest

model for the rotation of the Galaxy from Reid et al. 2014). These terms mostly cancel each other, so that the intrinsic spin-down, $\dot{P}_{\text{int}} = 2.8 \times 10^{-19} \text{ s s}^{-1}$, is very similar to the observed \dot{P} . This implies a low B-field of $\sim 5.8 \times 10^9 \text{ G}$ and a characteristic age of $\sim 6.7 \text{ Gyr}$. The origin of this pulsar is discussed in §4.

3 PULSE-SEQUENCE AND PROFILE ANALYSES AND QUANTITATIVE GEOMETRY

Recently, we conducted single-pulse polarimetric observations on most of the above pulsars as well as a few others of related interest. The Arecibo observations were carried out at both P band (327 MHz) and L band (1400 MHz) using total bandwidths of 50 MHz and typically 250 MHz, respectively. Four Mock spectrometers were used to sample adjacent subbands after MJD 56300 (see Mitra et al. 2016) and four Wideband Arecibo Pulsar Processors (WAPPs) earlier (Rankin et al. 2013) to achieve milliperiod resolution. The observations were then processed, calibrated and RFI

excised (e.g., see [Young & Rankin 2012](#)) to provide pulse sequences that were used both to compute average polarization profiles and fluctuation spectra. Rotation measures (RMs) were estimated for each of the pulsars by maximizing the linear polarization in the course of the polarimetric calibrations and analyses.

A summary of these polarimetric observations are given in Table 4, as described above. Nominal values of the rotation measure are also given in the table, and a complete description of the methods and errors will be given in a subsequent paper with many others. Below we treat the various pulsars object by object referring to the polarized profiles and fluctuation spectra in the Appendix figures. The analyses proceed from polarimetry to fluctuation spectra and finally to quantitative geometry following the procedures of [Rankin \(1993a,b\)](#). The longitude-resolved fluctuation (LRF) spectra of the pulse sequences (e.g., see [Deshpande & Rankin 2001](#)) were computed in an effort to identify subpulse “drift” or stationary modulation associated with a rotating (conal) subbeam system.

We have also attempted to classify the profiles where possible and conduct a quantitative geometrical analysis following the procedures of the core/double-cone model in [Rankin \(1993a,b\)](#); hereafter ET VI). Outside half-power (3-dB) widths are measured for both conal components or pairs—and where possible estimated for cores. Core widths can be used to estimate the angle between the rotation axis and magnetic axis α , polarisation position angle (PPA)-traverse central rates $R = \sin \alpha / \sin \beta$ can be used to compute β (the smallest angle between the magnetic axis and the line of sight), and the conal widths can be used to compute conal beam radii using eqs. (1) through (6) of the above paper.

The notes to Table 5 summarize our measurements, and the table values show the results of the geometrical model for the pulsar’s emission beams. The profile class is given in the first column, α and β in next two per the R value when possible. The conal component profile widths w , conal beam radii ρ , and characteristic emission heights h are tabulated in the rightmost three columns.

3.1 Analysis of Each Pulsar

J0435+2749 has a clear triple profile at both frequencies as shown in Figure 3, though the 1400 MHz profile is of better quality. The leading and trailing components have very different spectral indices: the trailing component is much stronger at 327 MHz, but the leading is much stronger at 1400 MHz. The fractional linear polarization is low in both profiles, and the PPA traverse is well defined only at the higher frequency. The power under the leading component may represent a different orthogonal polarization mode (OPM) than the others, suggesting little PPA rotation across the profile. Both fluctuation spectra show broad peaks at about 0.05 cycles/period, primarily in the two outer components, which suggest a 20-period conal modulation.

The observed conal spreading between the two frequencies suggests a core/outer cone beam geometry. The core width can only be estimated at the higher frequency at an upper limit of 9° implying that α is less than 1.4° per ET VIa, eq.(1).

The PPA traverse shows a much more complex behavior than the Rotation Vector Model (RVM) describes; however,

the roughly 90° rotation near the center of the pulse allows us to calculate the emission geometry using the RVM. The spherical geometric beam model in Table 5 seems compatible with a core-cone triple T classification.

J0517+2212 has a double component profile at 1400 MHz, whereas its 327 MHz profile shows some structure in the second component. The polarization traverse shows little rotation at 327 MHz apart from the two 90° “jumps” and the behaviour seems similar at 1400 MHz but less well resolved—perhaps because of the diminished fractional linear polarization. The fluctuation spectra shows a peak around 0.12 cycles/period, suggesting an 8 rotation-period modulation.

The increased structure at 1400 MHz, the overall pulse narrowing, and the lack of PPA traverse suggest that $\beta \sim 0$ and imply the outer conal beam geometry shown in Table 5.

J0627+0706 has a bright interpulse, separated from the main pulse by $177^\circ (\pm 0.27^\circ)$ as can be seen in Fig. 5. Because both features have structure, a more detailed interpretation is needed to assess how close to 180° they fall. However, given the narrowness of both features, it seems likely that they represent emission from the star’s two poles, implying an orthogonal geometry where α is close to 90° . PPA tracks give hints about the geometry only at 1400 MHz, and here little to go on apart from a probable 90° “jump” under the main pulse. The main pulse might have three components and the interpulse two. The fluctuation spectra are not displayed because they showed only flat “white” fluctuations.

The pulse width at half maximum widens from 327 MHz to 1400 MHz, suggesting a core-single configuration where the conal emission is seen mainly at high frequencies. The polarization traverse is clearer at 1400 MHz, marked by prominent 90° modal “jumps”. It thus seems likely that β is small for the main pulse and perhaps larger for the interpulse, but that α is close to 90° , yielding the classifications and model values in Table 5. The emission heights given for both the main pulse and interpulse suggest that it is inner conal emission.

J0927+2345 shows an interesting feature at 327 MHz approximately 180° away from the main pulse (Fig. 6). This apparent interpulse is discernible only in the 327 MHz profile, and disappears in the 1400 MHz profile. Again, both profiles show so little linear polarization that a reliable PPA rate can be estimated for only a narrow longitude interval at 327 MHz. The main pulse appears to have three closely spaced features. The fluctuation spectra are not given for this pulsar because they showed no discernible features.

The half width broadens from 327 MHz to 1400 MHz suggesting a core single evolution where conal “outriders” appear or become more prominent at high frequency. The polarization traverse is well defined only for a short interval at 1400 MHz, which provides a useful R value that leads to the geometric beam model in Table 5. If this profile were a triple, the central component would be 2.8° wide.

J0943+2253 nulls as seen in Fig. 1 above, but the fluctuation spectra show no quasiperiodic behavior. The linear polarization is slight and the PPA track shows what appears to be a 90° “jump” within the narrow interval where it is clearly defined.

The average 327 MHz profile has two closely spaced components and perhaps an unresolved weak feature on its

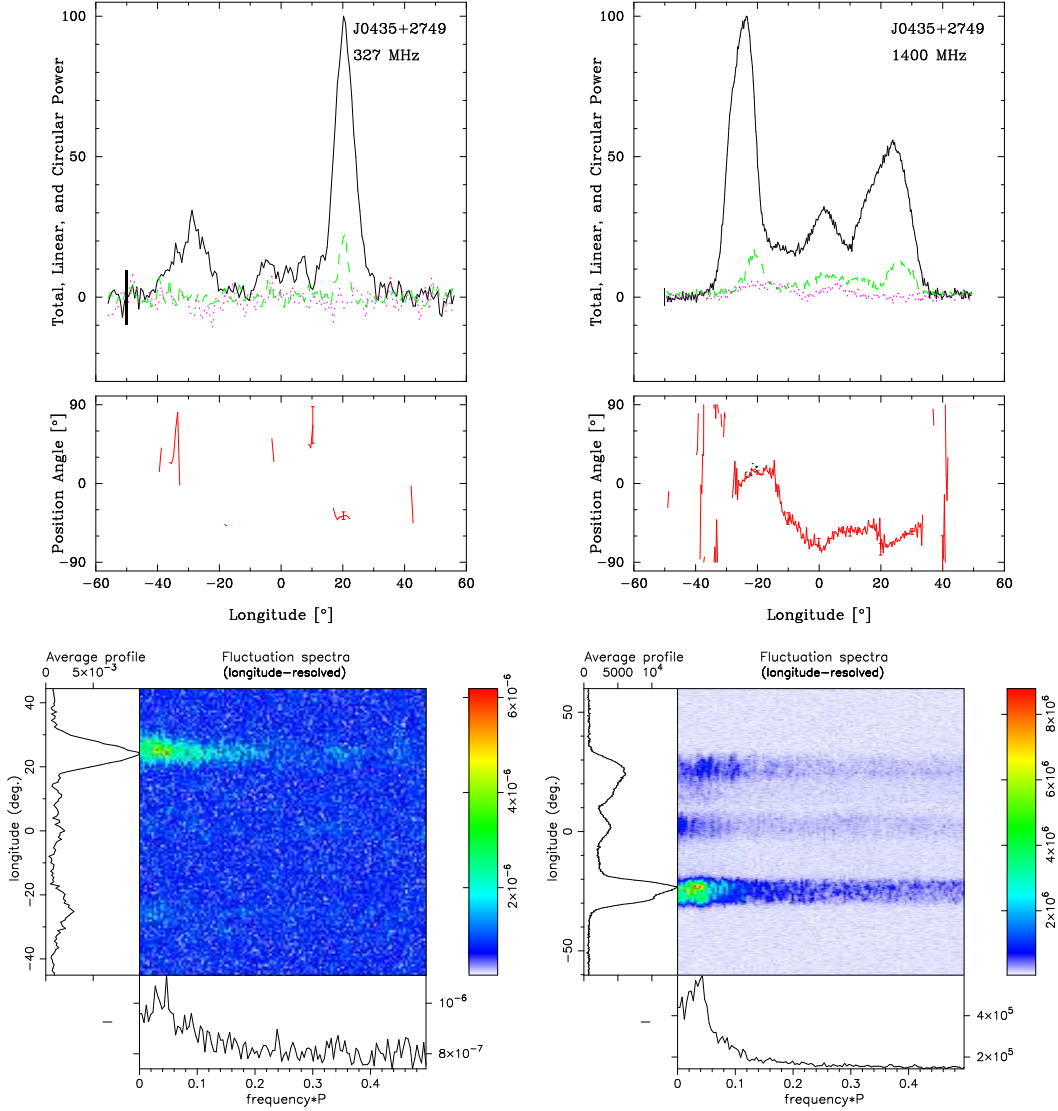


Figure 3. PSR J0435+2749 polarized profiles (upper displays) and fluctuation spectra (lower displays) at 327 MHz (left) and 1400 MHz (right). The upper panels of the polarization displays give the total intensity in mJy (Stokes I ; solid curve), the total linear (L ($=\sqrt{Q^2 + U^2}$); dashed green), and the circular polarization (Stokes V ; dotted red)—**with a righthand bar indicating 3- σ in the off-pulse noise level**. The PPA [$=(1/2)\tan^{-1}(U/Q)$] single values (dots, lower panels) in plots of the stronger pulsars correspond to those samples having errors smaller than 2σ in L , and the average PPA is over plotted (solid red curve) with occasional 3- σ errors. The longitude-resolved fluctuation spectra show the power levels (**arbitrary units**) in the main panel (**in cycles per rotation period**) according to the color bars (right). The average profiles are given in the left-hand panels and the aggregate fluctuating power in panels at the bottom of each display.

leading edge, suggesting a double or triple configuration. The 1400 MHz profile shows one main component, but there appears to be a bump on the leading edge indicating an additional component. The linear polarization is slight and difficult to interpret at 327 MHz, but is slightly more pronounced at 1400 MHz. We measure a central PPA rate of $7^\circ/\text{°}$ at both frequencies in order to compute the geometric model parameters in Table 5, which suggest an inner-conal configuration.

J0947+2740 shows three components at both frequencies, though the leading region may be more complex at the lower frequency, probably representing a core and closely spaced inner cone. At 1400 MHz the conal components are weaker,

and the PPA traverse is more complex. RVM behaviour and the slope of its polarization traverse could not be determined. This pulsar is also known to exhibit sporadic emission between intervals of weakness or nulls as in Fig. 1. The fluctuation spectra (not shown) seem to hint at fluctuation power at periods longer than about 3 or 4 pulses.

The fact that the profile width increases with wavelength indicates an outer-conal configuration. Its PPA traverse seems interpretable per the RVM model at 327 MHz, but its 1400 MHz traverse seems to be distorted by what may be a 90° “jump” just prior to the profile center. Its profile then seems to be a core/outer cone triple, and the quantitative beam geometry model is shown in Table 5. The

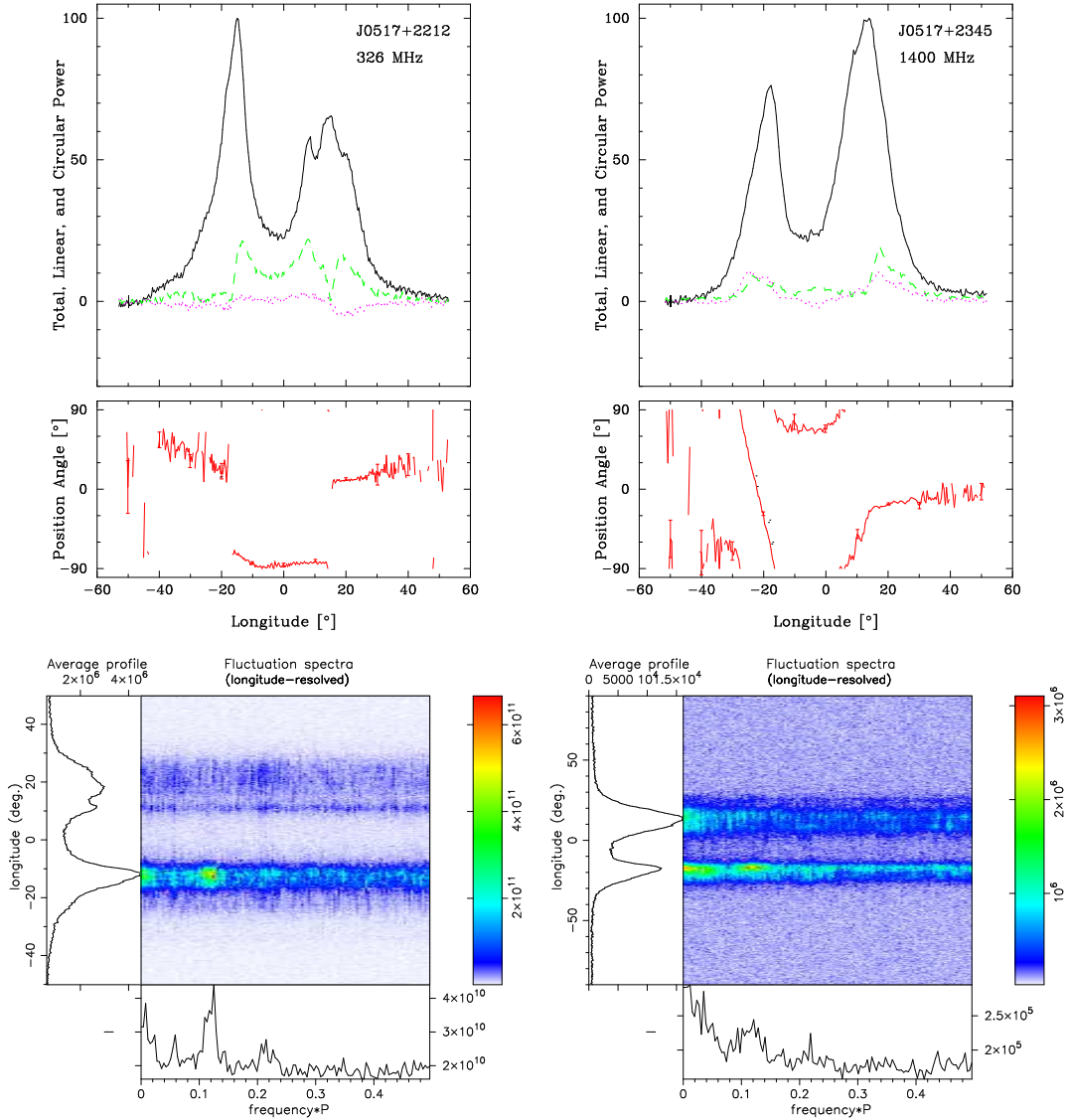


Figure 4. J0517+2345 polarized profiles and fluctuation spectra as in Fig. 3.

core width is estimated around 2.65° , which is much narrower than the central component of the profile (7.92° at 327 MHz and 10.08° at 1400 MHz); this indicates that the magnetic axis is canted at $42^\circ \pm 2.7^\circ$.

J1246+2253 has a single component at 327 MHz, which develops into a resolved triple form at 1400 MHz in what may be the characteristic core-single manner. The fractional linear polarization at both frequencies is low, so little can be discerned reliably from the PPA tracks. Also no clear features are seen in the fluctuation spectra as is often the case for core-single profiles.

The single profile at 327 MHz becoming triple at 1400 MHz strongly suggests a core-single configuration. Despite the low fractional linear polarization, the trailing positive traverse measured at 90° was used to compute the geometry in Table 5. The core width is calculated at 3.55° .

J1404+1159 exhibits a narrow peak in its fluctuation spectra around 0.2 cycles/period, suggesting a modulation period P_3 of some 5 rotation periods. A display of its individual

pulses bears this out, and a plot of its emission folded at P_3 shows that the modulation is highly regular. The PPA rate at the profile center suggests an outside sightline traverse as is usual for conal single “drifters”. See Figure 10.

The pulsar then appears to have a classic conal single profile. Both PPA tracks show a negative-going traverse with a central slope of $-12^\circ/^\circ$. Here we also give short pulse-sequences folded at the modulation period of some 0.2 rotation-periods/cycle.

J1756+1822 appears to have two profile components, and its profile broadens perceptibly with wavelength, suggesting a conal double configuration. Both frequency profiles have similar forms, with the longer wavelength profile somewhat broader in the usual pattern of the conal double class. The fractional linear profiles are low at both frequencies, but at 1400 MHz there seems to be a hint of a traverse through more than 90° across the profile. The fluctuation spectra are not shown as no features could be discerned.

J1935+1159’s long nulls (see Fig. 1) make this pulsar diffi-

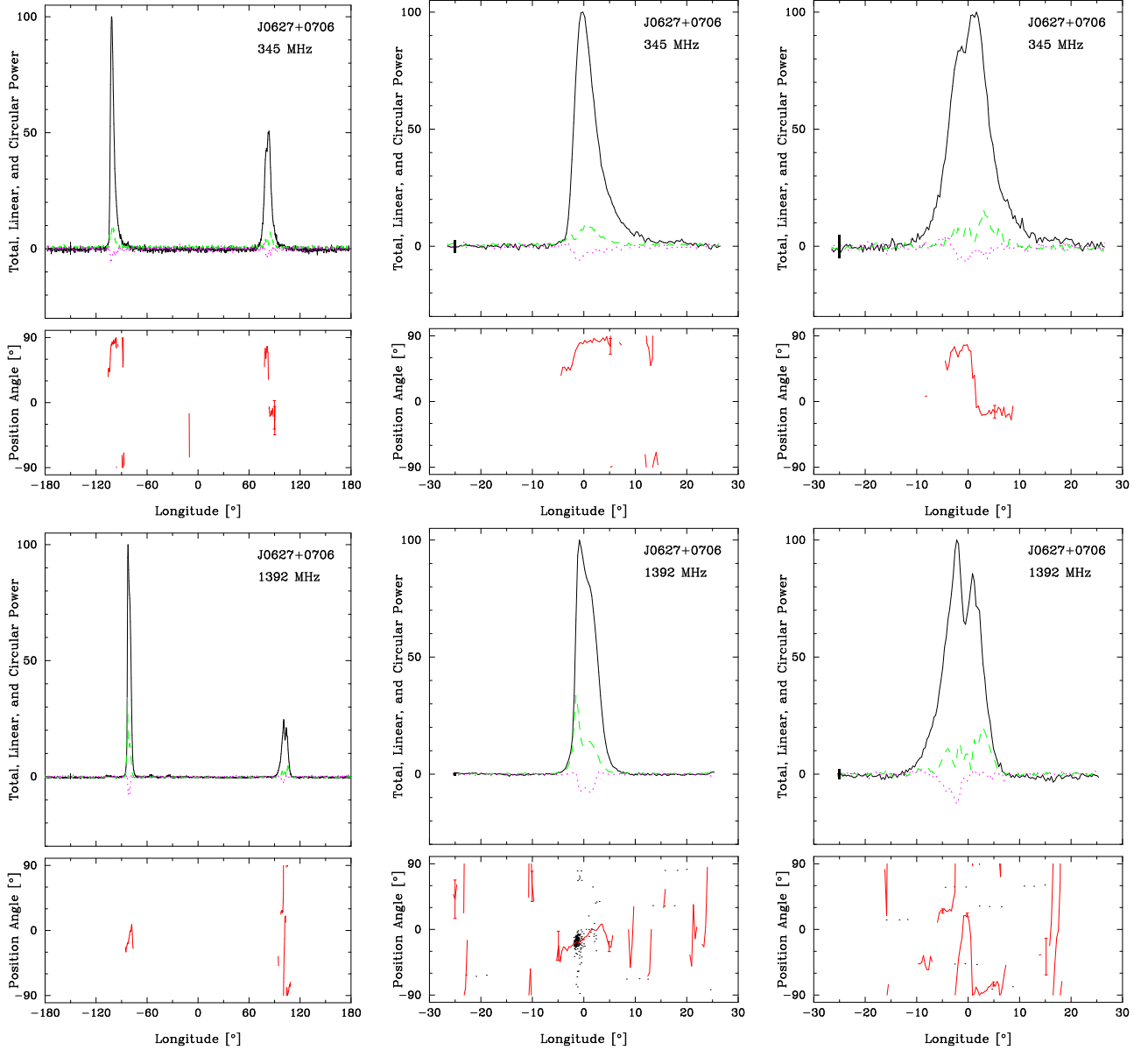


Figure 5. J0627+0706 327- (upper row) and 1400-MHz (lower row) MHz polarized profiles as in Fig. 3. Full period displays on the left show the pulsar’s main pulse and interpulse and the center and righthand plots show them separately.

cult to observe sensitively, and neither clear profile structure nor polarization signature is seen at either frequency. Similarly, fluctuation spectra showed nothing useful.

This appears to be a four or five component pulsar even though only three components can be resolved, it appears to have the central PPA traverse and usual filled “boxy” form which could hide additional components.

The emission heights, and the profile narrowing from 327 MHz to 1400 MHz, indicate that this is an outer cone which is filled with inner conal and/or core emission. For the geometric computations, we have estimated an unresolved central traverse of $10 \pm 2^\circ$.

J2050+1259 also exhibits frequent nulls as seen above in Fig. 1. However, its single profile at 1400 MHz broadens and

bifurcates at 327 MHz in the usual conal double manner, and a steep PPA traverse is seen at the lower frequency. Here we do see strong low frequency features in the fluctuation spectra indicative of modulation on a scale of 50 rotation periods or longer.

The profile has a single component at 1400 MHz and two closely spaced components at 327 MHz as seen in Figs. 1 and 13. Its profile is broader at the lower frequency, and strong hints of a $90\text{--}180^\circ$ PPA traverse are seen in both profiles, suggesting that this is a conal single profile with a small impact angle. Its beaming parameters are given in Table 5. **J2053+1718.** Our observations do not provide much polarization information or fluctuation-spectral information apart from it having a single profile at both frequencies. In the

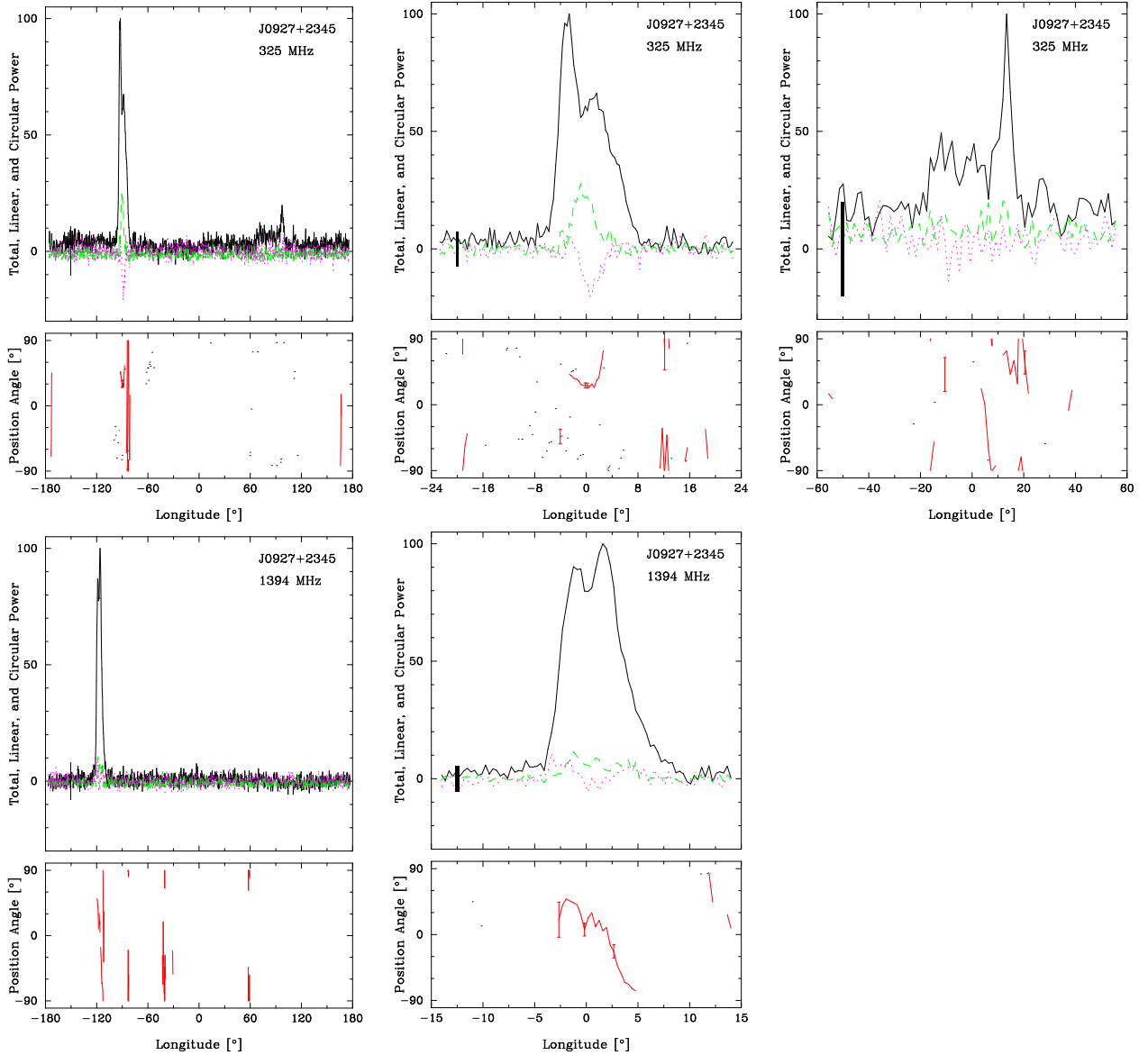


Figure 6. J0927+2345 as in Fig. 5. The pulsar’s weak interpulse was not detected at the higher frequency separately.

higher frequency observation the time resolution was poor with only 232 samples across the rotation cycle. This pulsar has a wider profile at 1400 MHz than at 327 MHz; however, we hesitate to make conclusions about profile measurements due to the low quality of the observation. Despite this, its short 119-ms rotation period and single profile do suggest a core-single classification.

4 ON THE ORIGIN OF PSR J2053+1718

In double neutron star systems, the first-born neutron star was recycled by accretion of mass from the progenitor of the second-formed neutron star. This accretion spun up the first formed NS to spin periods between 22 and 186 ms (for the

known DNSs, likely faster right after they formed) and, by mechanisms that are not clearly understood, it induced a decrease in its magnetic field to values between $10^9 < B_0 < 10^{10}$ G. Such pulsars spin down very slowly and therefore will stay in the active part of the $P - \dot{P}$ diagram for much longer than non-recycled pulsars; this is the reason why we mostly see the recycled pulsars in these systems (the second-formed non-recycled pulsars are observed in two DNSs only). For a review see [Tauris et al. \(2017\)](#).

Some isolated pulsars like PSR J2053+1718 are in the same area of the $P - \dot{P}$ diagram as the recycled pulsars in DNSs, but have no companion to explain the recycling. The conventional explanation for their formation is that, like the recycled pulsars in DNSs, they were spun up by a massive stellar companion; the difference is that when the latter star

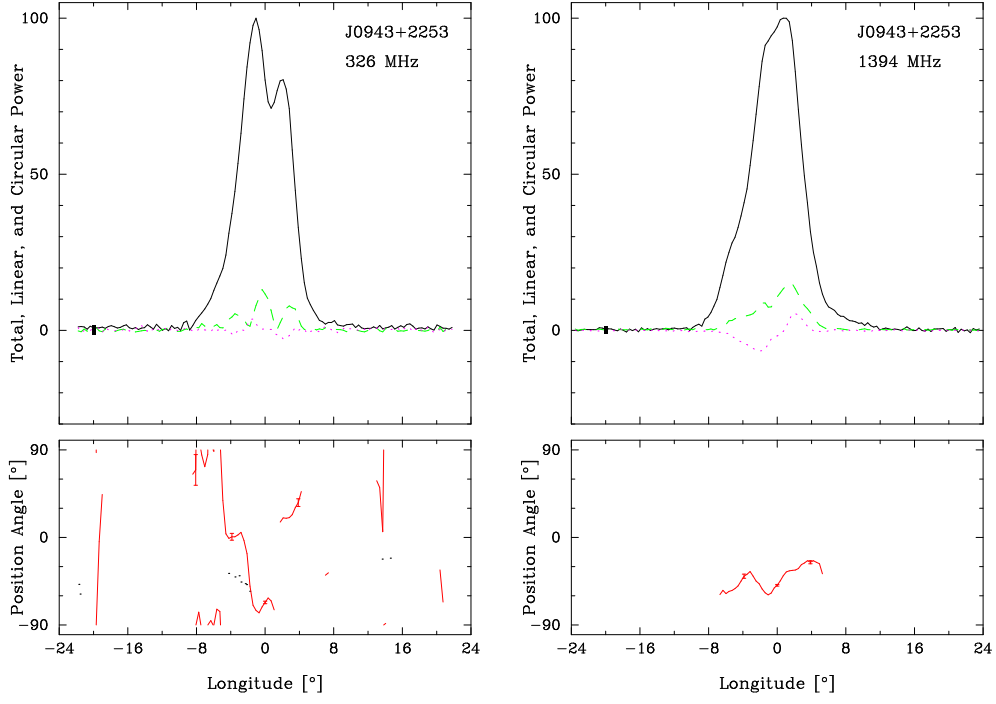


Figure 7. J0943+2253 polarized profiles as in Fig. 3.

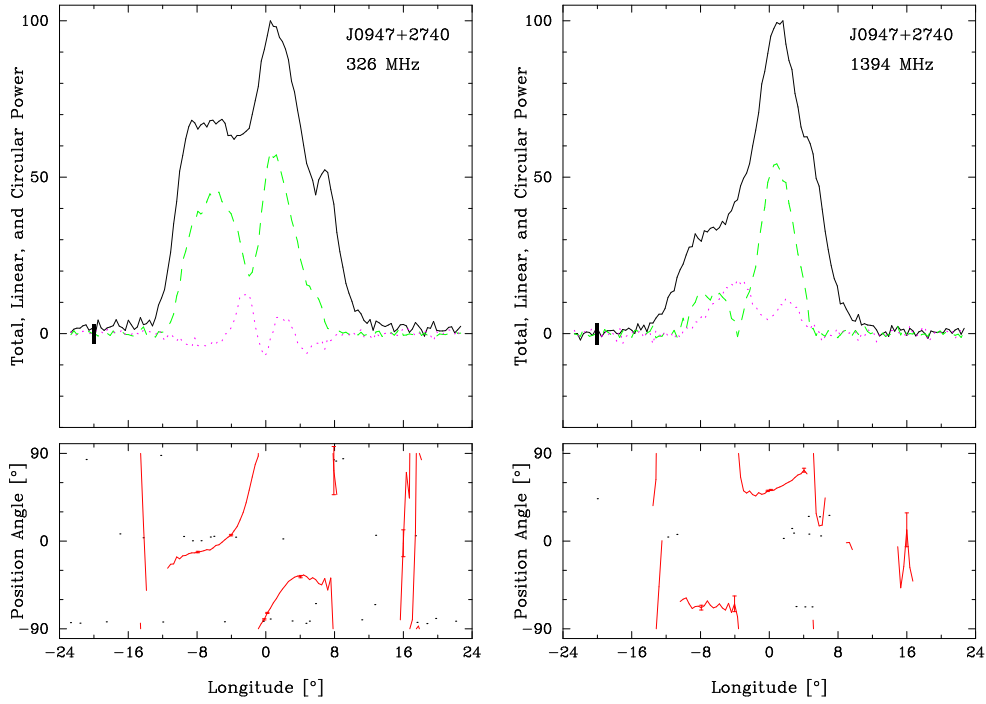


Figure 8. J0947+2740 polarized profiles as in Fig. 3.

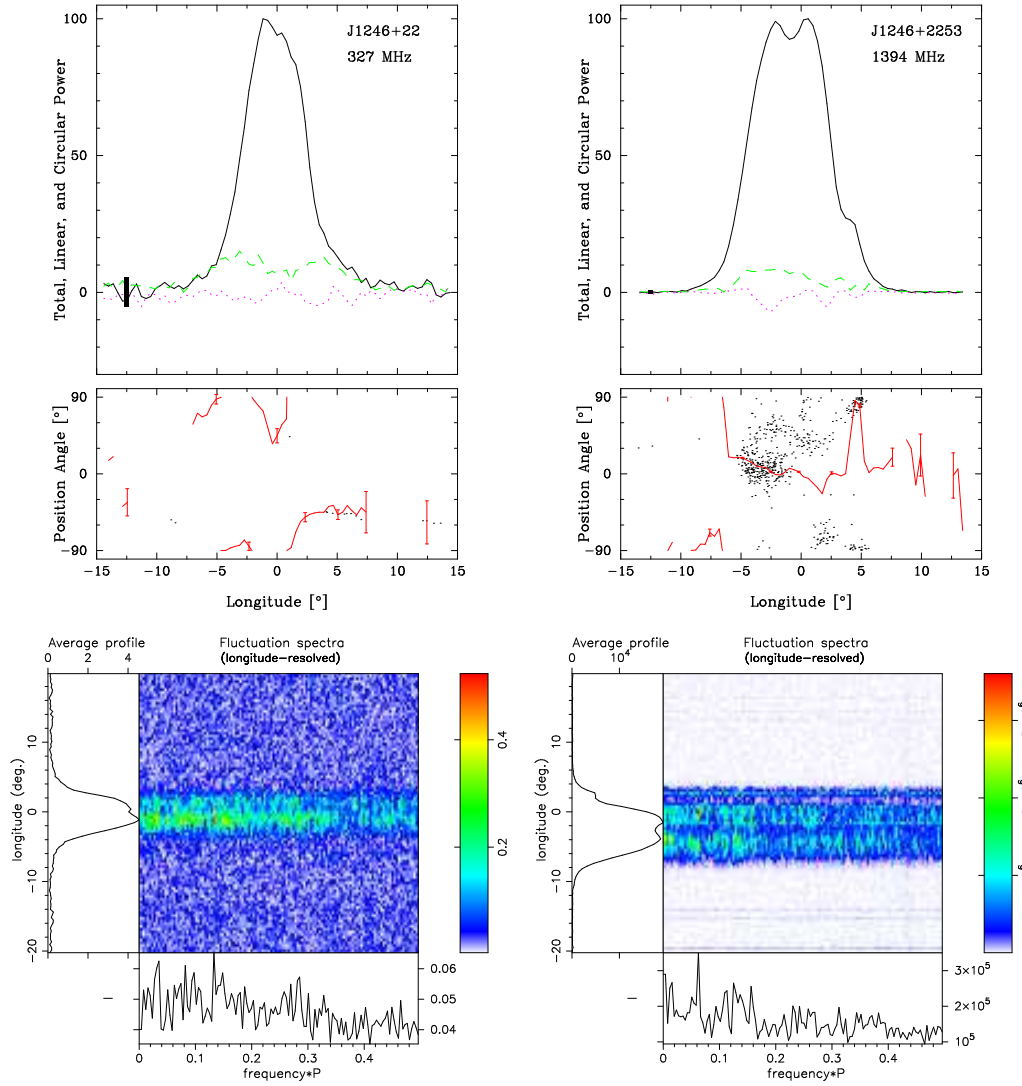


Figure 9. J1246+2253 polarized profiles and fluctuation spectra as in Fig. 3.

Name	MJD		Number of Pulses		Flux Density (mJy)		RM (rad-m ²)
	327 MHz	1400 MHz	327 MHz	1400 MHz	327 MHz	1400 MHz	
J0435+2749	56327	54541	1830	3065	3.4(4)	0.24(3)	+2
J0517+2212	57123	54540	2696	2698	3.4(1.5)	0.46(2)	-16
J0627+0706	57123	57113	518	2520	17(4)	1.0(1)	+212
J0927+2345	57525	57347	4724	2502	1.2(3)	0.06(1)	-8
J0943+2253	57379	57377	7775	13680	3.1(3)	0.39(7)	+8?
J0947+2740	57379	57524	3172	4699	2.3(3)	0.13(1)	+32
J1246+2253	56176	57307	1266	1885	2.4(7)	0.39(3)	+4?
J1404+1159	55905	57307	509	1591	4.3(9)	0.027(5)	+4
J1756+1822	57567	57567	2156	3571	<0.002	0.014(5)	+70
J1935+1159	57288	57533	1004	1090	1.5(9)	0.17(3)	-83
J2050+1259	57524	57525	2046	1966	2.6(6)	0.05(1)	-80
J2053+1718	57524	57533	5023	21624	4(2)	0.003(2)	-5

Table 4. Polarimetric observations.

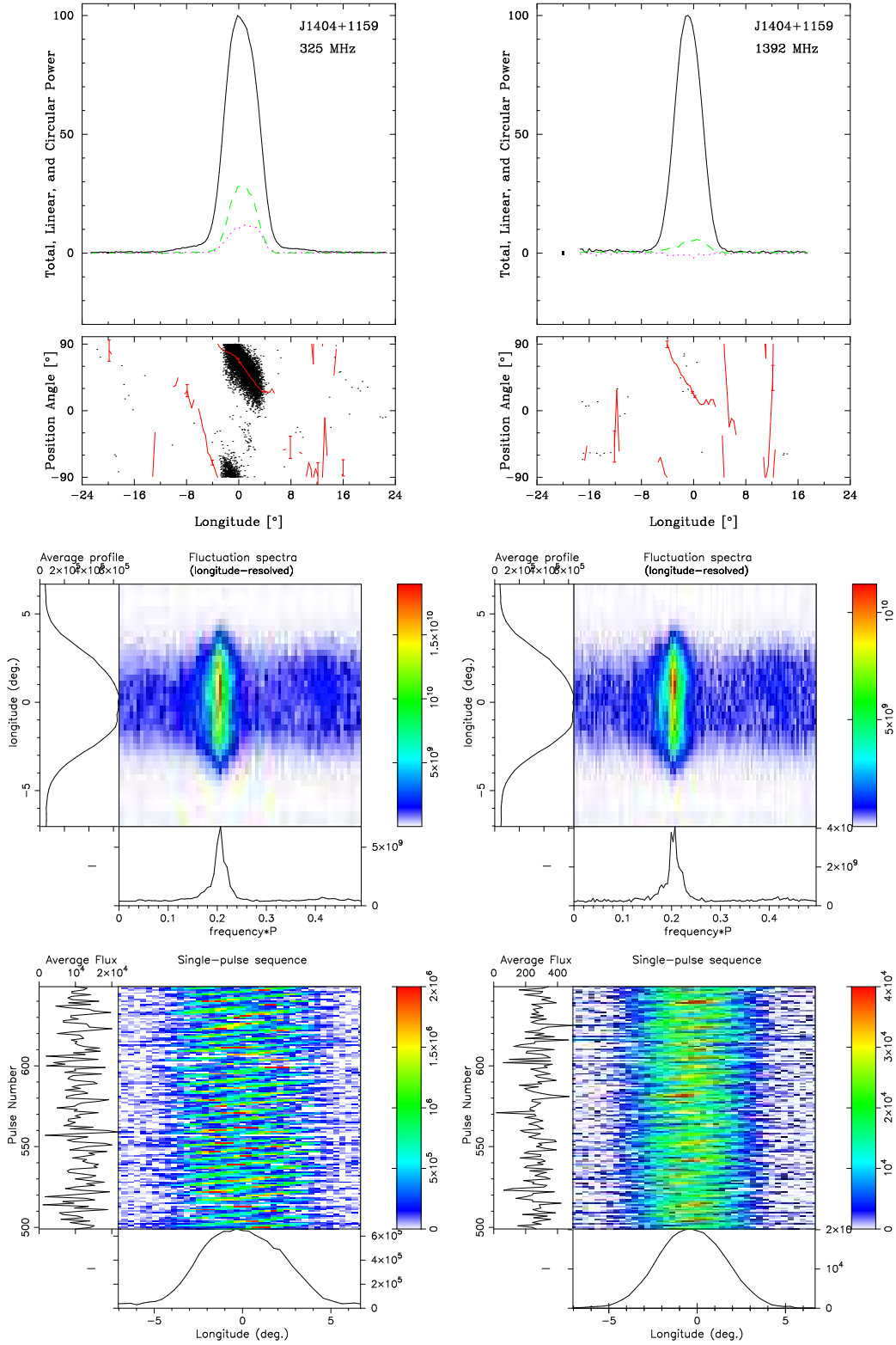


Figure 10. J1404+1159 polarized profiles and fluctuation spectrum as in Fig. 3. Additionally, a display showing the pulsar’s accurately drifting subpulses is given along the bottom.

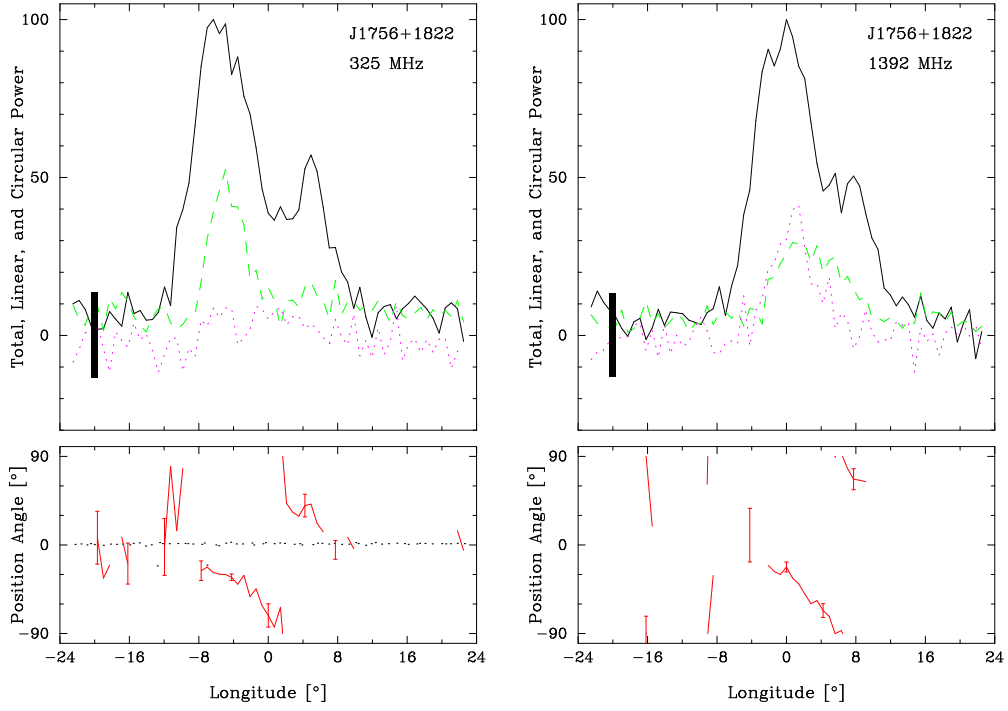


Figure 11. J1756+1822 polarized profiles as in Fig. 3.

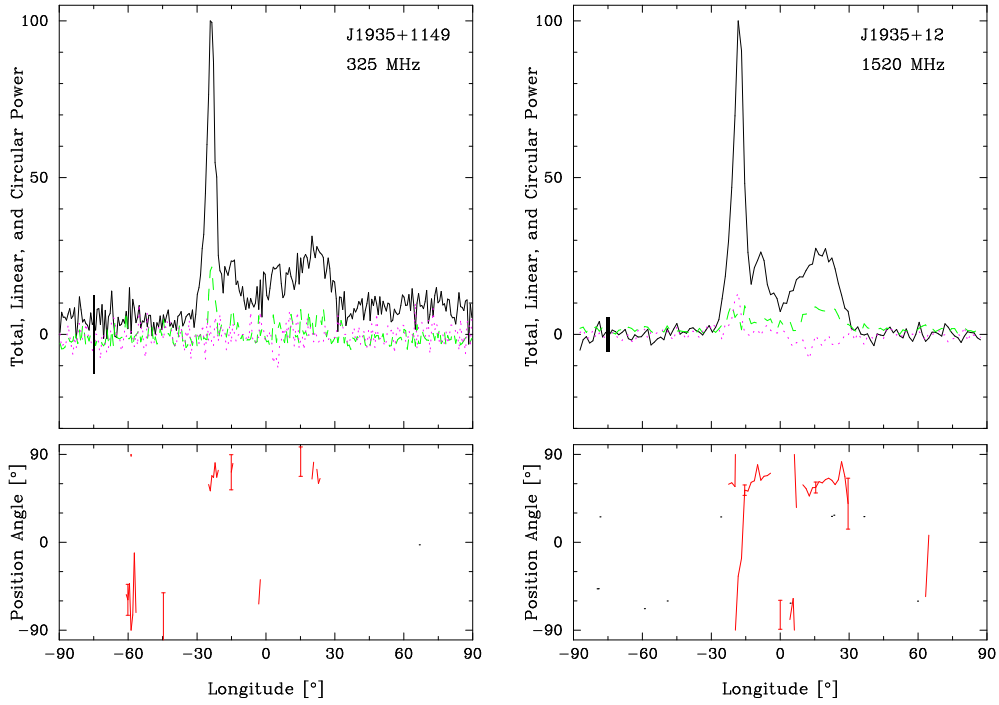


Figure 12. J1935+1159 polarized profiles as in Fig. 3.

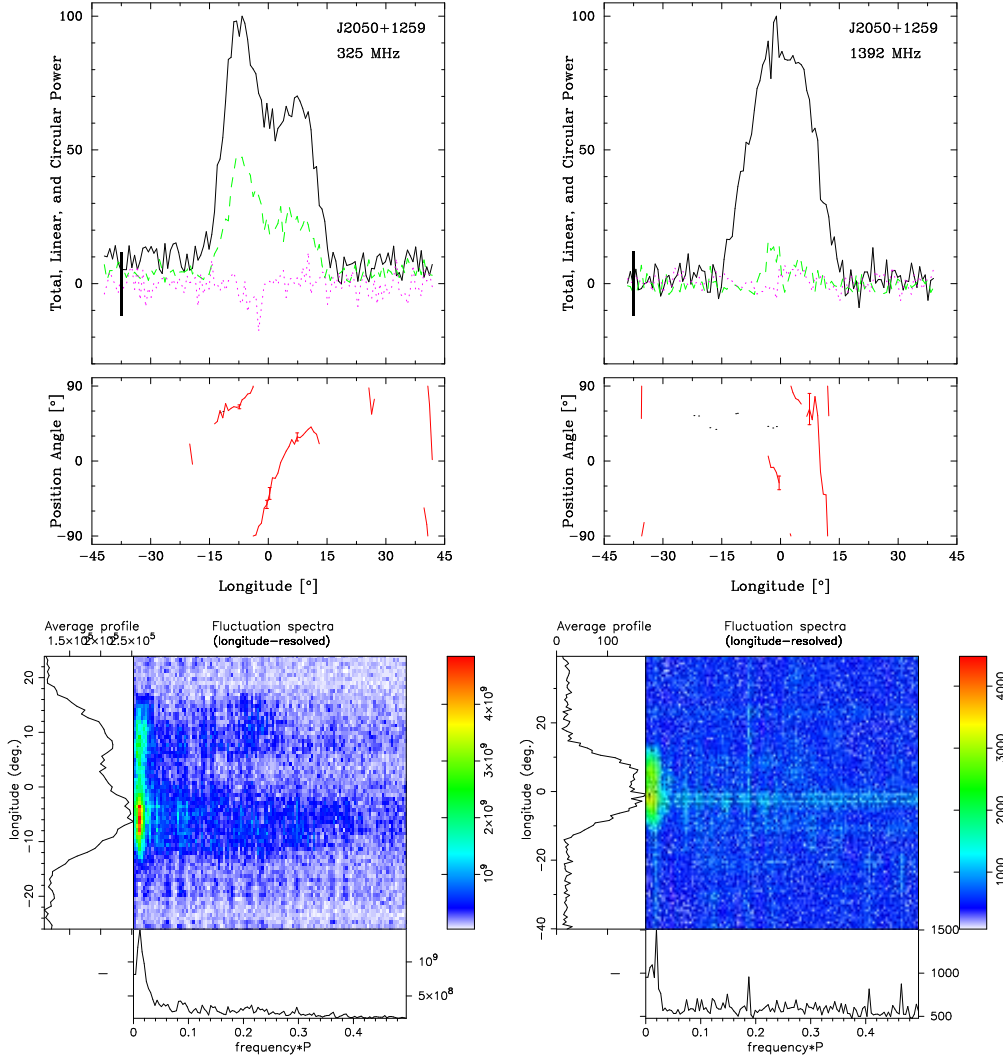


Figure 13. J2050+1259 polarized profiles and fluctuation spectra as in Fig. 3.

goes supernova and forms a neutron star, the system unbinds, owing to the kick and mass loss associated with the supernova (e.g., Belczynski et al. 2010). For this reason they have been labelled “Disrupted Recycled Pulsars”, or DRPs.

We should keep in mind the possibility of alternative origins for these pulsars: some NSs observed in the center of supernova remnants, despite being obviously young, have small B-fields and large characteristic ages similar to those of DRPs — these objects are known as Central Compact Objects, or CCOs (see e.g., Halpern & Gotthelf 2010). Therefore, one could expect that some DRPs formed as CCOs. However, Gotthelf et al. (2013) find after extensive study of DRPs in X-rays that none appears to have thermal X-ray emission, implying that there is likely no relation between CCOs and DRPs. This results in a mystery: a substantial fraction of neutron stars appear to form as CCOs, which one might reasonably expect to form DRP-like radio pulsars, some of them with strong thermal X-ray emission, but these large numbers of DRPs (and “hot” DRPs) are not ob-

served. Either, for some unknown reason, they never develop radio emission, or their B-field increases significantly after birth, making them look more like normal pulsars. In any case, the results of Gotthelf et al. (2013) seem to exclude the possibility that DRPs such as PSR J2053+1718 formed from central Compact Objects.

Any model that explains quantitatively the observed distribution of orbital eccentricities and spatial velocities of DNSs should also be able to explain the relative fraction of DRPs to DNSs and, furthermore, the velocity distribution of the two classes of objects. As already discussed by Belczynski et al. (2010), the relative number of DNSs and DRPs implies that the second SN kick must be, on average, significantly smaller than that observed for single pulsars. The evidence for this among DNSs has been growing in recent years and is now very strong (see comprehensive discussion in Tauris et al. 2017). It is therefore clear that more measurements of proper motions, spin periods, ages and B-fields of

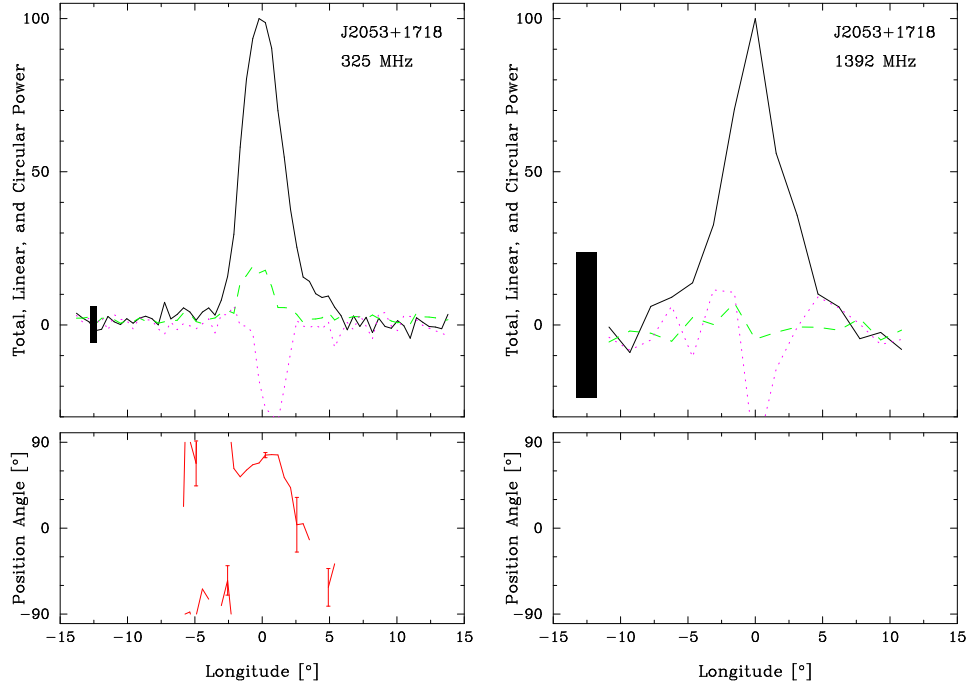


Figure 14. J2053+1718 polarized profiles as in Fig. 3.

Pulsar	Class	w_{327} (°)	w_{1400} (°)	α (°)	β (°)	w (°)	ρ (°)	h (km)	R (°/°)	Notes
J0435+2749	T	63.0	59.0	18	+3.4	59.0	10.3	230	5	
J0517+2212	D	55.0	45.5	31	0	45.2	11.7	205	6	Both frequencies have a flat PPA traverse, suggesting central sightline, $\beta \sim 0^\circ$
J0627+0706m	S_t	4.5	4.5	90	-7.2	4.5	7.5	131	8	
J0627+0706i	D	6.0	6.0	90	-6.4	6	6.9	129	9	178° apart from main pulse.
J0927+2345m	D/T?	5.0	6.4	69	+3.4	8	5.1	130	16	
J0943+2253	D/T?	6.5	7.8	42	-5.5	7	5.9	123	7	R was measured at 327 MHz.
J0947+2740	T/M	19.4	17.0	42	-1.2	18	6.0	205	32	Core widths: $\sim 8^\circ, 10^\circ$ at 327, 1400 MHz
J1246+2253	S_t	5.7	7.4	81	-4.7	6.5	5.7	103	12	
J1404+1159	S_d	5.8	5.0	25	+2.2	5.3	0.88	114	11	
J1756+1822	D	16.0	15.3	50	+2.5	16	6.7	224	18	Core widths: $8.2^\circ, 7.1^\circ$ at 327, 1400 MHz. R was measured at 1400 MHz.
J1935+1159	D	51.8	50.5	10.13	-1.0	50.4	4.3	239	10	
J2050+1259	S_d	25.0	18.0	27	-2.6	21	5.2	223	10	R measured at 327 MHz
J2053+1718	$S_t?$	2.5	5.0	63	-17.2	2.5	17.2	235	16	

Table 5. Conal Geometry Models. The profile classes are defined in Rankin (1993a). w_{327} and w_{1400} represent the half-power pulse widths (in degrees) at 327 and 1400 MHz respectively. α values are estimated from core component widths per ET VIa, eq.(1) where possible and β from eq.(3). The outer half-power widths w are interpolated to 1 GHz from profile measurements, and then ρ and h computed using eqs.(4) and (6). R is the polarization position angle slope. (a) No data available for PSR J0943+2253 at 1400 MHz.

DRPs such as those presented here give us important clues for understanding the formation of DNS systems.

5 CONCLUSIONS

In the foregoing sections we have characterized a group of pulsars that had not been the target of any previous detailed

studies. We determined timing solutions for them; most are normal, isolated pulsars. One of them, PSR J0627+0706, is relatively young ($\tau_c = 250$ kyr) and is located near the Monoceros SNR, however it is unlikely that the pulsar and that SNR originated in the same supernova event: We find that a nearby “radio quiet” pulsar recently discovered by the Fermi satellite, PSR J0633+0632, is located closer to

the centre of the cluster and has a characteristic age that agrees better with the estimated age of the SNR.

We confirmed a candidate from a previous survey, PSR J2053+1718; subsequent timing shows that, despite being solitary, this object was recycled; it appears to be a member of a growing class of objects that appear to result from the disruption of double neutron stars at formation. We highlight that measurements of the characteristics of these objects (spin period, age, B-field, velocity) are important for understanding the formation of double neutron star systems.

As part of our characterization, we have also observed these pulsars polarimetrically with the Arecibo telescope at both 1400 MHz and 327 MHz in an effort to explore their pulse-sequence properties and quantitative geometry. Three of them (PSRs J0943+2253, J1935+1159 and J2050+1259) have strong nulls and sporadic radio emission, several others exhibit interpulses (PSRs J0627+0706 and J0927+2345) and one shows regular drifting subpulses (J1404+1159). All these measurements will contribute to future, more global assessments of the emission properties of radio pulsars and studies of the NS population in the Galaxy.

ACKNOWLEDGMENTS

Much of the work was made possible by support from the US National Science Foundation grant 09-68296 as well as NASA Space Grants. One of us (JMR) also thanks the Anton Pannekoek Astronomical Institute of the University of Amsterdam for their support. Arecibo Observatory is operated by SRI International under a cooperative agreement with the US National Science Foundation, and in alliance with SRI, the Ana G. Méndez-Universidad Metropolitana, and the Universities Space Research Association. This work made use of the NASA ADS astronomical data system. One of us (KS) thanks the US National Science Foundation for their support under the Physics Frontiers Center award number 1430284.

REFERENCES

- Abdo A. A., et al., 2009, *Science*, **325**, 840
 Belczynski K., Lorimer D. R., Ridley J. P., Curran S. J., 2010, *MNRAS*, **407**, 1245
 Burgay M., et al., 2013, *MNRAS*, **429**, 579
 Chandler A. M., 2003, PhD thesis, California Institute of Technology
 Cordes J. M., Lazio T. J. W., 2002, arXiv:astro-ph/0207156,
 Damour T., Taylor J. H., 1991, *ApJ*, **366**, 501
 Demorest P. B., et al., 2013, *ApJ*, **762**, 94
 Deneva J. S., Stovall K., McLaughlin M. A., Bates S. D., Freire P. C. C., Martinez J. G., Jenet F., Bagchi M., 2013, *ApJ*, **775**, 51
 Deshpande A. A., Rankin J. M., 2001, *MNRAS*, **322**, 438
 Dowd A., Sisk W., Hagen J., 2000, in Kramer M., Wex N., Wielebinski R., eds, *Astronomical Society of the Pacific Conference Series Vol. 202, IAU Colloq. 177: Pulsar Astronomy - 2000 and Beyond*. pp 275–276
 Gonzalez M. E., et al., 2011, *ApJ*, **743**, 102
 Gotthelf E. V., Halpern J. P., Allen B., Knispel B., 2013, *ApJ*, **773**, 141
 Halpern J. P., Gotthelf E. V., 2010, *ApJ*, **709**, 436

- Hewish A., Bell S. J., Pilkington J. D. H., Scott P. F., Collins R. A., 1968, *Nature*, **217**, 709
 Leahy D. A., Naranan S., Singh K. P., 1986, *MNRAS*, **220**, 501
 Lorimer D. R., Kramer M., 2004, *Handbook of Pulsar Astronomy*
 Lorimer D. R., Camilo F., McLaughlin M. A., 2013, *MNRAS*, **434**, 347
 Manchester R. N., Hobbs G. B., Teoh A., Hobbs M., 2005, *AJ*, **129**, 1993
 Mitra D., Rankin J., Arjunwadkar M., 2016, *MNRAS*, **460**, 3063
 Navarro J., Anderson S. B., Freire P. C., 2003, *ApJ*, **594**, 943
 Odegard N., 1986, *ApJ*, **301**, 813
 Rankin J. M., 1993a, *ApJS*, **85**, 145 (ET VIa)
 Rankin J. M., 1993b, *ApJ*, **405**, 285 (ET VIb)
 Rankin J. M., Wright G. A. E., Brown A. M., 2013, *MNRAS*, **433**, 445
 Ransom S. M., Eikenberry S. S., Middleditch J., 2002, *AJ*, **124**, 1788
 Ray P. S., Thorsett S. E., Jenet F. A., van Kerkwijk M. H., Kulkarni S. R., Prince T. A., Sandhu J. S., Nice D. J., 1996, *ApJ*, **470**, 1103
 Ray P. S., et al., 2011, *ApJS*, **194**, 17
 Reid M. J., et al., 2014, *ApJ*, **783**, 130
 Shklovskii I. S., 1970, *Soviet Ast.*, **13**, 562
 van Straten, W., Demorest, P., & Osłowski, S. 2012, *Astronomical Research and Technology*, **9**, 237
 Tauris, T. M., Kramer, M., Freire, P. C. C., et al. 2017, *ApJ*, **846**, 170
 Taylor J. H., 1992, *Philosophical Transactions of the Royal Society of London Series A*, **341**, 117
 Thorsett S. E., Deich W. T. S., Kulkarni S. R., Navarro J., Vasishth G., 1993, *ApJ*, **416**, 182
 Yao J. M., Manchester R. N., Wang N., 2017, *ApJ*, **835**, 29
 Young S. A. E., Rankin J. M., 2012, *MNRAS*, **424**, 2477

This paper has been typeset from a \TeX/L\AA\TeX file prepared by the author.